

Electrochemical Investigation on Shielding Effect of Crevice Structure in Bridge Concrete on Cathodic Protection

Juanling Wang*, Mengshi Wang

Yellow River Conservancy Technical Institute, Kaifeng 475004, China

*E-mail: teacher_wang126@126.com

Received: 7 April 2022 / Accepted: 10 May 2022 / Published: 6 June 2022

In the bridge concrete, reinforcement corrosion is one of the main factors affecting the service life and safety performance of bridges, in which cathodic protection (CP) technology is widely used in the corrosion protection of reinforcement in bridge concrete. However, exposed in the atmosphere for a long time, there are much more crevices in the bridge concrete, which will greatly shorten the protection distance of cathodic current, and then aggravate the corrosion of reinforcement in the crevices. Therefore, based on the self-designed rectangular crevice structure as the experimental device to simulate the crevices in the bridge concrete, this paper studied the corrosion behavior of HRB500 steel inside and outside the crevice structure in 3 wt.% NaCl solution under the different conditions of CP current densities through electrochemical experiments and corrosion morphology characterization. The results showed that under the condition of no cathodic protection, the crevice corrosion mechanism generally changed from activation corrosion to oxygen concentration corrosion with the increase of experimental time, presenting that the self-corrosion potential of the HRB500 steel inside the crevice structure positively shifted, while the self-corrosion potential of the HRB500 steel outside the crevice structure shifted first to positive direction and then to negative direction. When cathodic protection was applied, the corrosion behaviors of the HRB500 steels along the crevice structure were all showed in activation corrosion, and the corrosion behavior of HRB500 steel outside the crevice was transformed from anode control to mixed control, and from general corrosion to pitting corrosion. Under the conditions of increasing CP current densities, the corrosion behavior was depended on cathodic process with a decreasing cathodic Tafel constant (β_c), while the corrosion morphology changed from pitting corrosion to general corrosion.

Keywords: Electrochemical experiment; Bridge concrete; HRB500 reinforcement; Cathodic protection

1. INTRODUCTION

The deterioration of reinforced concrete structure of bridge is the synergistic result of physical - chemical process. Compared with freeze-thaw damage and alkali-aggregate reaction, reinforcement corrosion is the main reason of durability decline of concrete structures [1-4]. The corrosion will lead to the reduction of the cross-sectional area of reinforcement, which will greatly reduce the load capacity of the bridge, resulting in a significant decrease in service life of the bridge [1,2,4-6]. This phenomenon is particularly obvious in the pre-stressed reinforced concrete structures eroded by Cl^- [1, 5, 6].

Nowadays, cathodic protection (CP) technology has been widely used for reinforcement anti-corrosion in bridge concrete, and has been proved by corrosion scientists to be the best way to prevent Cl^- corrosion in the reinforced concrete structure [7-9]. For example, the British Standards Organization pointed out that CP was the only way to protect reinforcements from chloride ions in concrete structures [10,11]. The American Concrete Institute also came up with that only CP had proven to be the most effective method of preventing the continued Cl^- erosion of existing concrete structures [12,13].

Two reported cases can prove the effectiveness of CP in the anti-corrosion of reinforcements in bridge concrete. In 2013, Christodoulou et al. [14] applied a hybrid CP system on the Tiwai Point Bridge to provide anti-corrosion for pre-stressed concrete in the tidal zone with a target service life of 50 years. In 2014, Christodoulou et al. [15] conducted a study and analysis on the CP of bridge in Midland, and found that after CP was applied in 1987, the Cl^- corrosion of the bridge was greatly reduced. Since then, CP had been the main anti-corrosion method for MLMV bridges, including more than 740 concrete structures currently protected by CP.

However, exposed in the atmosphere for a long time, crevices inevitably occurred in the bridge concrete at the interface between concrete and reinforcements, which can shield the CP current. Under this circumstance, the corrosion rate of reinforcements in the crevice structure can reach 0.7 mm/a. As shown in Figure 1, during the on-site inspection of reinforcement corrosion, it was found that under the condition of CP potential of -1.1~-1.2 V (relative to the saturated copper sulfate reference electrode, vs.CSE), the crevices formed at the interface of concrete and reinforcements had a shielding effect on CP current, that is, the distance of CP was shortened due to the crevices [16]. The micro corrosion morphology of the reinforcements in the protected area and unprotected area was carried out, as shown in Figure 2. It can be seen that the corrosion of reinforcements in protected area was very slight, and it can be considered to be well protected. However, due to the shielding effect of the crevice structure on the CP current, the reinforcements inside the crevice structure were not protected, so the corrosion was serious, and there were a lot of pits on the surface.

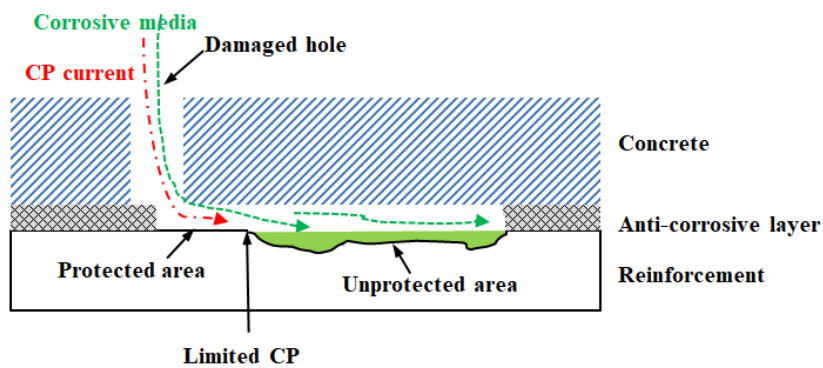


Figure 1. The shielding effect of crevice structure in on-site bridge concrete on CP current

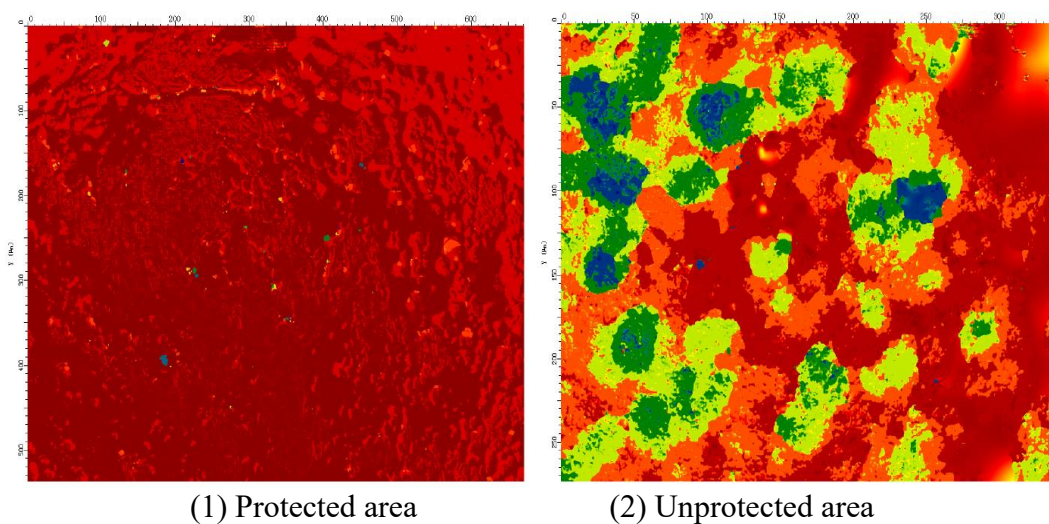


Figure 2. The micro corrosion morphology of the reinforcements in bridge concrete in protected area and unprotected area under the condition of CP potential of $-1.1 \sim -1.2 \text{ V}_{\text{vs.CSE}}$

Therefore, based on the self-designed rectangular crevice structure as the experimental device to simulate the crevice structure in the bridge concrete, this paper studied the corrosion behavior of HRB500 reinforcement inside and outside the crevice structure in 3 wt.% NaCl solution under different conditions of CP current densities (I_{CP}) in $0\text{-}100 \text{ A/cm}^2$ through electrochemical experiments and corrosion morphology characterization, to reveal the shielding effect of the crevice structure in bridge concrete on CP and corrosion behaviors of metal inside the crevice structure in the bridge concrete.

2. EXPERIMENTAL SETUPS

2.1 Self-corrosion potential of HRB500 steel in the crevice structure with time

In order to explore the variation of the self-corrosion potential (E_{sc}) of HRB500 steel along the crevice structure in bridge concrete with time, as shown in Figure 3, the rectangular structure as

experimental device was used to simulate the crevice structure in bridge concrete for experimental testing. The upper and lower cover plates of the experimental device were made by poly ethylen material, and four locations for test samples were preset in the lower cover plate. 1# sample was set at the position of the openings, at which the test sample was in direct contact with the external corrosive environment, and was not influenced by the crevice structure. And the 2#, 3# and 4# samples were set at positions 3 cm, 9 cm and 15 cm away from the 1# sample. A reference electrode (saturated calomel electrode, SCE) was set at the upper cover corresponding to each test sample. The potentiometer was used to collect the potential of the four samples, and the potential acquisition of different samples could be carried out by switching data acquisition unit. NaCl solution with a mass fraction of 3% was used as the experimental solution, the experimental temperature was 20°C, and the total experimental time was set as 144 h. HRB500 steel with the size of 7×7×2 mm³ was used for the experiments, and the main components were shown in Table 1. Before the experiment, each sample should be cleaned and polished to be mirror-like.

Table 1. The main chemical components of HRB500 steel (mass fraction, wt.%)

Element	C	Si	Mn	P	S	Ceq
Mass fraction (%)	0.22	0.54	1.41	0.036	0.040	0.48

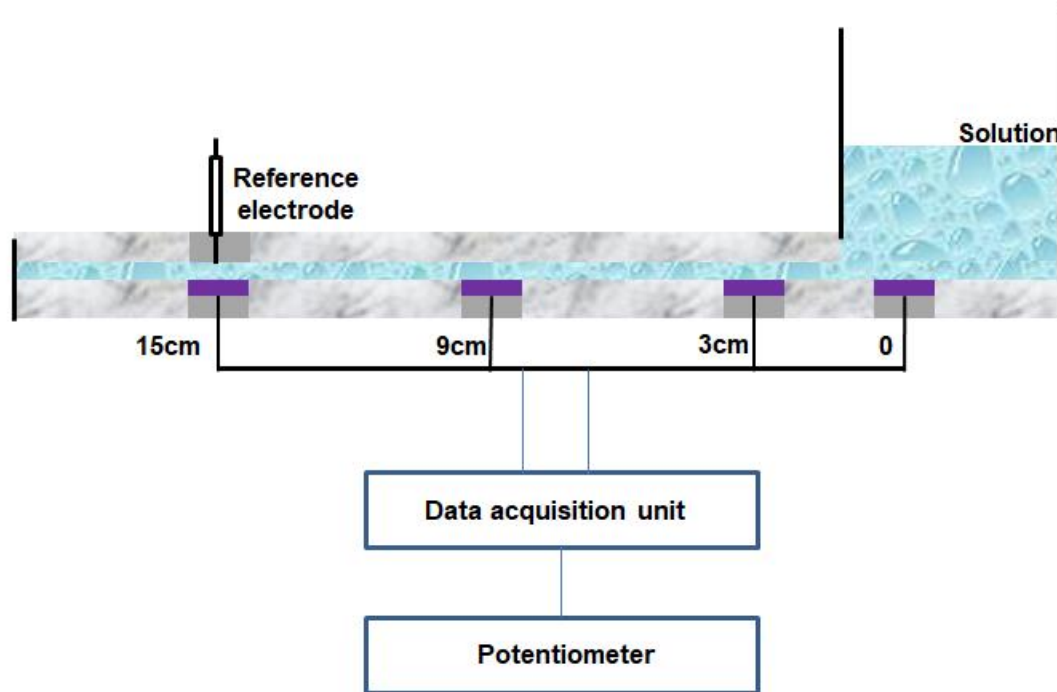


Figure 3. The rectangular structure as the experimental device for simulating the crevice structure in bridge concrete to test the self-corrosion potential (E_{sc}) of HRB500 steel obtained by data acquisition unit and potentiometer at different position (0, 3 cm, 9 cm and 15 cm away from the opening, named 1#-4# sample, respectively) with time in 3 wt.% NaCl solution at 20°C

2.2 Shielding effect of the crevice structure on cathodic protection

On the basis of experimental device as shown in Figure 3, a platinum electrode (Pt) was added close to each reference electrode to test the polarization curves of the different samples, as shown in Figure 4. The CP of the 1# sample was applied by the direct current (DC) source, to simulate the different CP degrees, where the anode was Pt electrode and the cathode was the 1# sample. The I_{CP} was set in the range of 0-100 A/m². After the system was stabilized, the polarization curves of 1# and 4# samples were tested to analyze the shielding effect of the crevice structure on CP under different conditions of I_{CP} . The polarization curve was scanned in Tafel potential range and the scanning rate was set as 0.1 mV/s.

The immersion tests of 1# and 4# samples under different conditions of I_{CP} were set for 72 h. After completed, the sample was removed to clean the surface corrosion products, and the corrosion morphology was observed with a 3D microscope and then the maximum pit depth was tested.

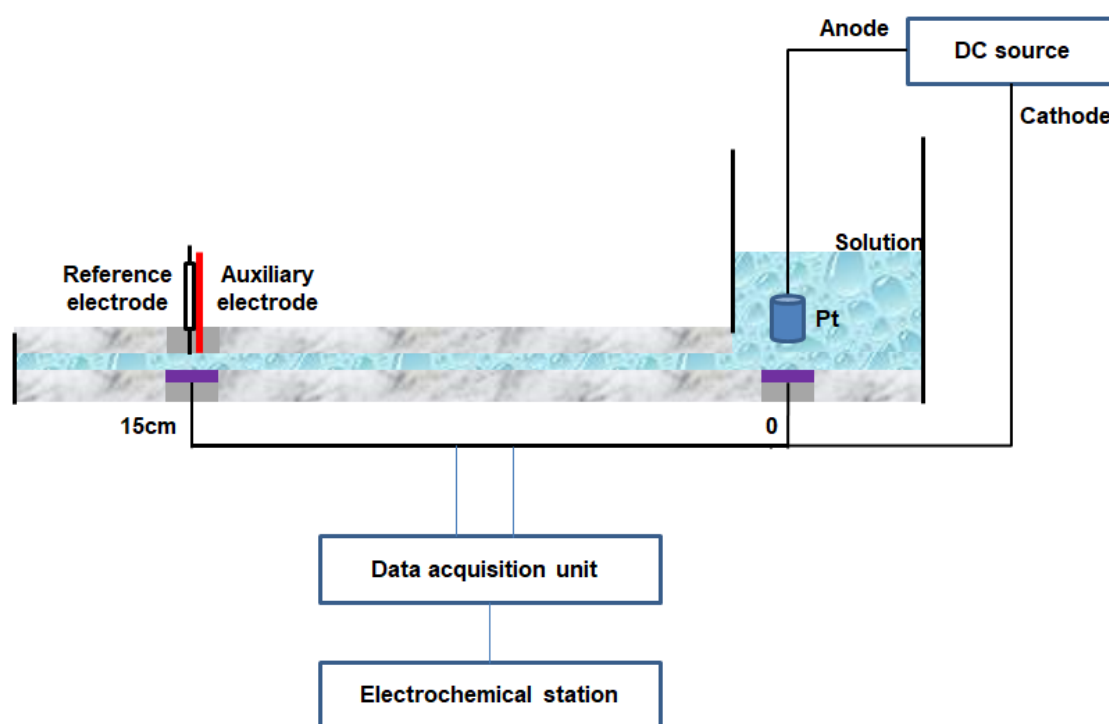


Figure 4. The rectangular crevice structure as the experimental device for simulating the crevice structure in bridge concrete to carry out the electrochemical experiments and immersion experiments (including corrosion morphology and maximum pitting depth) of HRB500 steel at different positions of 1# and 4# samples, respectively, with time in 3 wt.% NaCl solution at 20°C under the different conditions of cathodic potential current densities in the range of 0-100 A/m²

3. RESULTS AND DISCUSSION

3.1 Self-corrosion potential of HRB500 steel in the crevice structure under the condition of no cathodic protection with time

Figure 5 showed the variation of self-corrosion potential (E_{sc}) of four samples at different positions with experimental time of 0-144 h. As can be seen from the Figure 5, the variation of E_{sc} of different samples can be divided into two stages of 0-36 h and 36-144 h. In the first stage of 0-36 h, with the increase of the experimental time, the E_{sc} of different samples was all positively shifted, indicating an intensified corrosion. Therefore, the activation corrosion of HRB500 steel occurred in this stage. This was because at the initial stage (0-36 h) of the experiment, the electrochemical reaction in the crevice structure was controlled by the oxygen depolarization with the sufficient oxygen, that is, $Fe \rightarrow Fe^{2+} + 2e^-$ in the anode and $O_2 + 2H_2O + 4e^- \rightarrow 4OH^-$ in the cathode. And also, the corrosion product $Fe(OH)_2$ was in a loose porous structure, which can further promote the adsorption of anions on the surface of the metal matrix [17]. Therefore, in the first stage of 0-36 h, the E_{sc} of HRB500 steel was positively shifted with time increasing.

However, in the second stage of 36-144 h, the E_{sc} of different samples showed different changes compared with that in 0-36 h. In detail, the E_{sc} of 1# and 2# samples close to the opening gradually shifted negatively with the increase of experimental time, while the E_{sc} of 3# and 4# samples continued to shift positively and then remained basically unchanged. Meanwhile, it should be noted that within 36-72 h, the E_{sc} of different samples presented obvious positive or negative deviation. However, at 72-144 h, the E_{sc} of 2#, 3# and 4# samples basically remained unchanged, while the E_{sc} of 1# sample continued to deviate slightly in negative position. Therefore, when the experimental time reached 144 h, comparing the E_{sc} of different samples, it can be seen that 3# and 4# samples were worked as anode, while 1# and 2# samples were worked as cathode [18-20]. This was because as the experiment progressed, the oxygen inside the crevice structure was gradually consumed. However, due to the shielding effect of the crevice structure, the oxygen outside the crevice structure was difficult to diffuse into the crevice structure, so the oxygen concentration difference gradually increased [21]. As a result, within 36-72 h, the E_{sc} of 1# and 2# samples were negatively shifted, while the E_{sc} of 3# and 4# samples continued to show positive deviation. When the difference of oxygen concentration along the crevice structure reached equilibrium [22], the E_{sc} of different samples remained basically unchanged after 72 h.

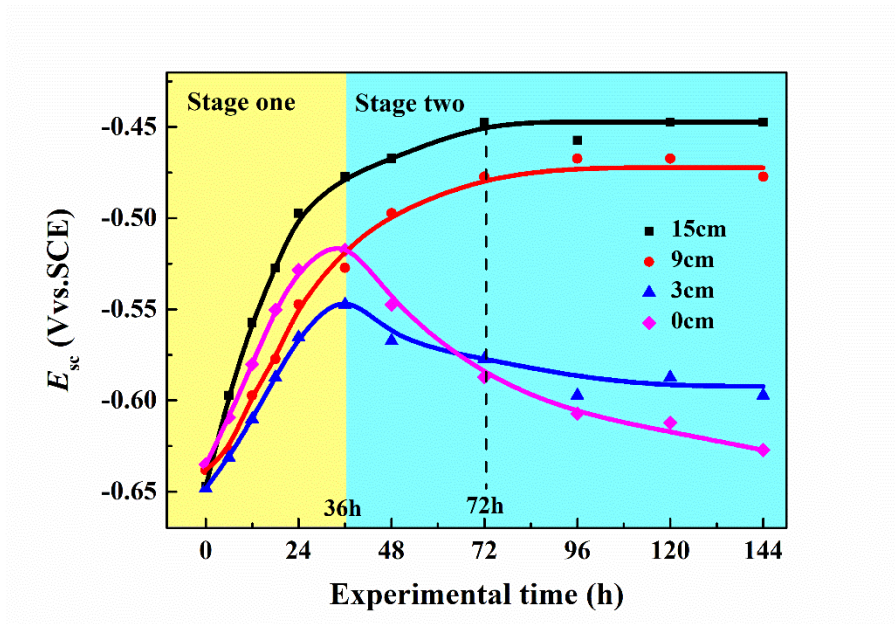


Figure 5. The variation of self-corrosion potential (E_{sc}) of four samples at different positions under the condition of no cathodic protection with time in 3 wt.% NaCl solution at 20°C

3.1 Self-corrosion potential of HRB500 steel in the crevice structure under the different conditions of CP current densities in 0-100 A/m²

Figure 6 showed the variation of self-corrosion potential (E_{sc}) of 1# sample under different conditions of CP current densities (I_{CP}) in 0-100 A/m² in 3 wt.% NaCl solution at 20°C. After CP was applied, the E_{sc} of HRB500 steel decreased from -647.23 mV to -1158.25 mV at $I_{CP} = 20$ A/m². As the I_{CP} continued to increase, the E_{sc} accordingly continued to shift negatively. When the I_{CP} reached 100 A/m², the E_{sc} moved negatively to -1592.17 mV. It should be noted that when the I_{CP} was 20 A/m² and 40 A/m², the E_{sc} was -1158.25 mV and -1186.34 mV, respectively, which can be considered within the admittedly effective range of CP potential in -0.85~ -1.2 V (relative to saturated copper sulfate electrode, CSE). Actually, more examples of CP applied on bridge concrete indicated the CP potential at the negative feedback point was generally set to -1.5 V to ensure that the CP current can protect much longer bridge [23]. And for another aspect, related studies had shown that for HRB500 steel, when the potential of uncoated metal in seawater was negative to -1.2 V, hydrogen-evolution reaction (HER) may occur, resulting in further deterioration of reinforcement. However, the HER of coated reinforcements in the bridge did not occur at the higher CP potential in -1.5 V. Therefore, under the condition of the applied I_{CP} in this study, the E_{sc} of HRB500 steel in $I_{CP} = 20$ -100 A/m² was basically equal to the CP potential actually set in the field.

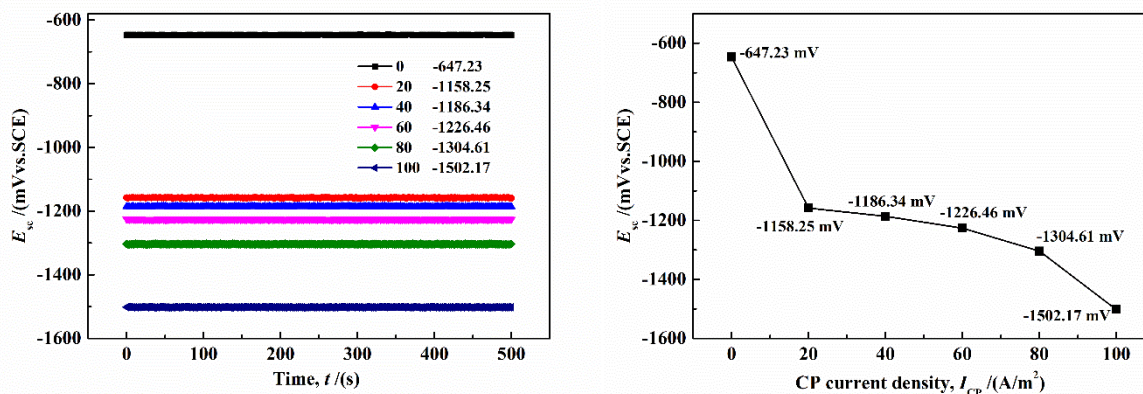


Figure 6. The variation of self-corrosion potential (E_{sc}) of 1# sample under the different conditions of CP current densities in 0-100 A/m² with time in 3 wt.% NaCl solution at 20°C

Figure 7 showed the variation of self-corrosion potential (E_{sc}) of 4# sample under the different conditions of CP current densities (I_{CP}) in 0-100 A/m² with time in 3 wt.% NaCl solution at 20°C. It was well-known that the more I_{CP} was impressed, the more negative of potential of protected metal was. However, in this paper, due to the shield effect of crevice structure on CP, it can be seen that with the increase of I_{CP} , the E_{sc} of 4# sample tended to increase, which was similar with the change mechanism of the anodic current outflowing from the metal. According to Faraday's law, under the condition of anodic current, the positive deviation of metal potential should be proportional to the anodic current. However, under the research conditions of this paper, as the I_{CP} increased, the increase rate of E_{sc} gradually slowed down, presenting a power exponential change of E_{sc} vs. I_{CP} ($R^2=0.998$) [24]. This was because that as shown in Figure 5, under the condition of no cathodic protection, the crevice corrosion mechanism was described by 1# sample as cathode and 4# sample as anode. However, due the shield effect of crevice structure on cathodic protection, that is, the applied CP current can not reach the 4# position, the applied CP made the potential difference severe increase (as shown in Figure 6 and Figure 7), which sharply accelerated the corrosion rate of 4# sample. A large number of Fe^{2+} at 4# position were accumulated due to the accelerated $Fe \rightarrow Fe^{2+} + 2e^-$, and then the Fe^{2+} hydrolysis process of $Fe^{2+} + 2H_2O \rightarrow 2H^+ + Fe(OH)_2$ led to the acidification of corrosion environment. Under this circumstance, due to the balance of positive - negative charges, a large amount of Cl^- migrated from 1# position to 4# position, resulting in increase in the local corrosion on the surface of 4# sample and then exacerbating the non-Faraday process [25]. Therefore, the change of E_{sc} vs. I_{CP} was in a power exponential function, rather than in a linear relationship.

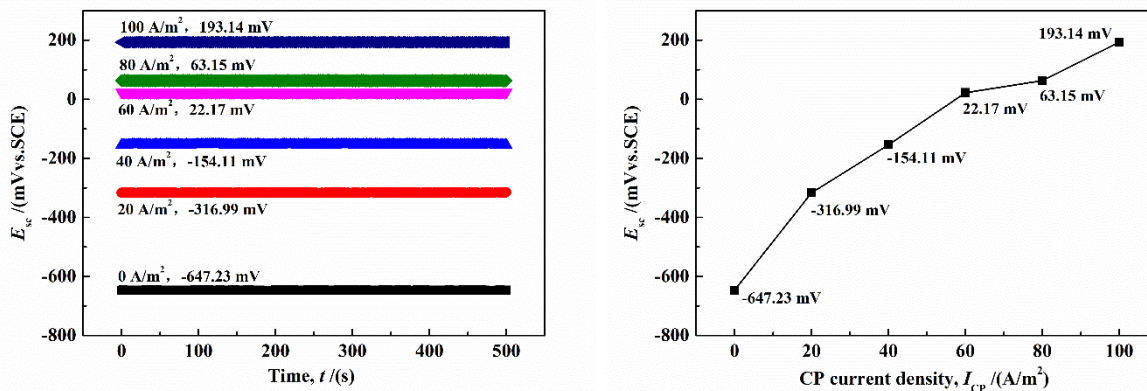


Figure 7. The variation of self-corrosion potential (E_{sc}) of 4# sample under the different conditions of CP current densities in 0-100 A/m² with time in 3 wt.% NaCl solution at 20°C

3.2 Polarization curves of HRB500 steel in the crevice structure under the different conditions of CP current densities in 0-100 A/m²

Figure 8 showed the variation of polarization curves and related parameters of 1# sample under different conditions of CP current densities (I_{CP}) in 0-100 A/cm² in 3 wt.% NaCl solution at 20°C, and Table 2 presented the fitted results of related parameters including corrosion potential (E_{corr}), corrosion current density (I_{corr}) and anode / cathode Tafel constant (β_a and β_c). As can be seen from the Figure 8, with the increase of I_{CP} , the E_{corr} of 1# sample continued to shift negatively. Especially, the change of E_{corr} was the largest, reaching 554.02 mV, when the $I_{CP} = 20$ A/m² was applied, which was the same as the result of self-corrosion potential (E_{sc}). Meanwhile, the I_{corr} showed a trend of firstly decreasing and then increasing. Under the different conditions of I_{CP} , the corrosion behavior of 1# sample presented an activation corrosion characteristic and was controlled by anode reaction presented by $r > 1$. However, the variation of r was contrary to that of I_{corr} , showing a trend of firstly increasing and then decreasing [26]. The larger the r was, the stronger the anode control effect was, and the more difficult ion diffusion was, so the lower I_{corr} was. Therefore, at $I_{CP} = 20$ A/m² and 40 A/m², the anode control was the strongest and the I_{corr} was relatively lower. However, with the increase of I_{CP} , the anode control weakened and tended to be mixed control ($r = \beta_a / \beta_c \approx 1$), resulting in that the I_{corr} increased gradually. This was because the HER potential of HRB500 steel in seawater (or 3.0-3.5 wt.% NaCl solution) was about -1.2 V. With the increase of I_{CP} , the E_{corr} of 1# sample was negative to the HER potential. Under this circumstance, the HER occurred, and the degree of anode control was weakened. As a result, the I_{corr} , namely the corrosion rate, increased.

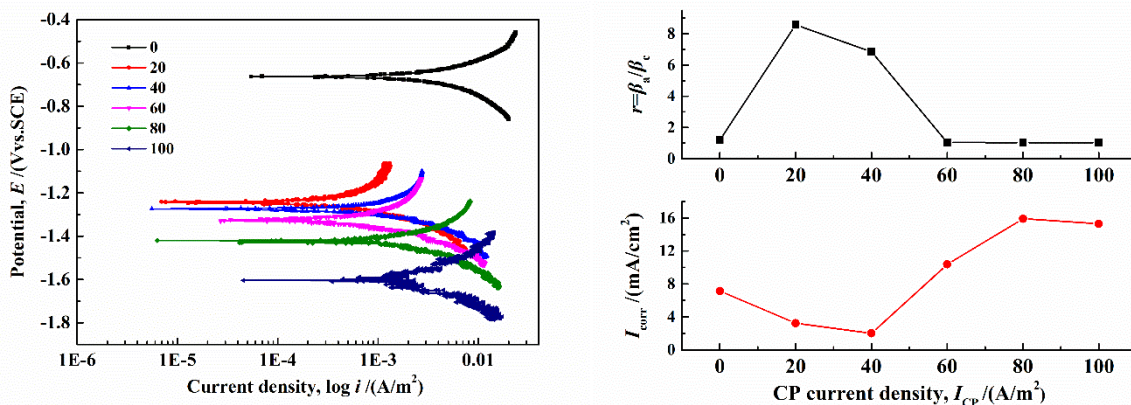


Figure 8. The variation of polarization curves and related parameters including corrosion current density (I_{corr}) and anode / cathode Tafel constant (β_a and β_c) of 1# sample under different conditions of CP current densities in 0-100 A/cm² in 3 wt.% NaCl solution at 20°C

Table 2. The fitted results of related parameters including corrosion potential (E_{corr}), corrosion current density (I_{corr}) and anode / cathode Tafel constant (β_a and β_c) of 1# sample under different conditions of CP current densities in 0-100 A/cm² in 3 wt.% NaCl solution at 20°C

CP current densities (A/m ²)	0	20	40	60	80	100
E_{corr} (mV)	-687	-1241	-1279	-1336	-1429	-1607
I_{corr} (mA/cm ²)	7.14	3.24	2.01	10.38	15.91	15.30
β_a (mV/dec)	1697.88	555	407.38	59.3	192.04	448.12
β_c (mV/dec)	1415.82	64.66	59.5	56.91	186.61	433.74
$r = \beta_a/\beta_c$	1.20	8.58	6.85	1.04	1.03	1.03

Figure 9 showed the variation of polarization curves and related parameters of 4# sample under different conditions of CP current densities (I_{CP}) in 0-100 A/cm² in 3 wt.% NaCl solution at 20°C, and Table 3 presented the fitted results of related parameters. Under the different conditions of I_{CP} applied on 1# sample, the corrosion behavior of 4# sample showed in an activation state, in which there were no passivation characteristics in anodic zone and no oxygen-diffusion characteristics in cathodic zone. With the increase of I_{CP} , the E_{corr} of 4# sample showed an obvious positive deviation. Meanwhile, the I_{corr} increased rapidly, but deviated slightly from the positive proportion trend, which was caused by the non-Faraday process described in Figure 7 [27]. The Tafel constant ratio ($r = \beta_a/\beta_c$) showed that the corrosion behavior of 4# sample changed from anodic control ($r > 1$) at $I_{CP} = 0$ to cathodic control ($r < 1$) in $I_{CP} = 20-100$ A/m². Furthermore, the r decreased gradually, which indicated that the larger I_{CP} applied on 1# sample was, the stronger the shielding effect of crevice structure on cathodic protection was. As a result, the I_{corr} basically increased linearly.

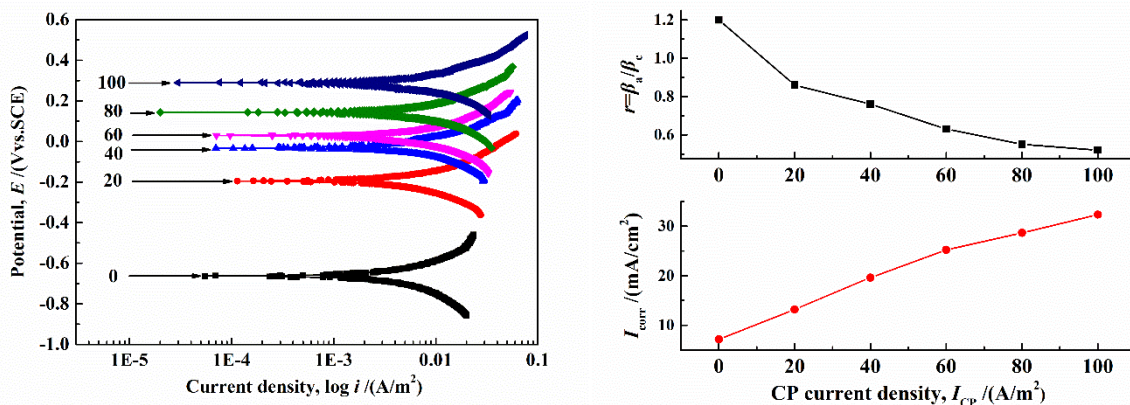


Figure 9. The variation of polarization curves and related parameters including corrosion current density (I_{corr}) and anode / cathode Tafel constant (β_a and β_c) of 4# sample under different conditions of CP current densities in 0-100 A/cm² in 3 wt.% NaCl solution at 20°C

Table 3. The fitted results of related parameters including corrosion potential (E_{corr}), corrosion current density (I_{corr}) and anode / cathode Tafel constant (β_a and β_c) of 4# sample under different conditions of CP current densities in 0-100 A/cm² in 3 wt.% NaCl solution at 20°C

CP current densities (A/m ²)	0	20	40	60	80	100
E_{corr} (mV)	-687	-353	-196	-37	36	160
I_{corr} (mA/cm ²)	7.14	13.18	19.61	25.20	28.66	32.36
β_a (mV/dec)	1697.88	920.3	401.85	426.84	1058.32	520.48
β_c (mV/dec)	1415.82	1074.75	531.87	674.42	1914.91	1001.92
$r = \beta_a / \beta_c$	1.20	0.86	0.76	0.63	0.55	0.52

3.3 Corrosion morphology and maximum pitting depth of HRB500 steel in the crevice structure under the different conditions of CP current densities in 0-100 A/m²

Figure 10 showed the corrosion morphology and maximum pitting depth of 1# and 4# samples under different conditions of CP current densities (I_{CP}) in 0-100 A/cm² in 3 wt.% NaCl solution at 20°C.

With the increase of I_{CP} , the corrosion morphology of 1# sample changed from general corrosion to pitting corrosion, and the area of corrosion pitting gradually increased. The results of maximum pitting depth showed that at $I_{CP} = 40$ A/m², the maximum pitting depth was 92.843 μm. With the continuous increase of I_{CP} , the maximum pitting depth was basically unchanged with an average of 96.034 μm, which was caused by the HER. In detail, under the condition of $I_{CP} = 20$ and 40 A/m², the E_{sc} of 1# sample was -1158.25 mV and -1186.34 mV, respectively, which was in acceptable CP potential range of -0.85~-1.2 V. Under this condition, the corrosion was been inhibited. However, the E_{sc} moved negatively to be lower than -1.2 V, the HER occurred, resulting in severe pitting corrosion. Therefore, in $I_{CP} = 40-100$ A/m², the HER was the main reaction of 1# sample, so the maximum pitting depth of HRB500 steel was basically unchanged.

Meanwhile, when the CP was applied on 1# sample, the corrosion characteristic of 4# sample showed obvious pitting characteristics. At $I_{CP} = 40 \text{ A/m}^2$, the maximum pitting depth reached $104.255 \mu\text{m}$. As the I_{CP} continued to increase, the area of corrosion pitting of 4# sample gradually increased, while the maximum pitting depth gradually decreased, which was $51.271 \mu\text{m}$ at 100 A/m^2 . This was because due to the shielding effect of crevice structure on cathodic protection, the larger the I_{CP} applied on 1# sample was, the higher potential difference of 1# and 4# samples was, in which the 4# sample worked as anode. The accelerated anodic reaction made the accumulation of corrosion products on the surface. For another aspect, the loose corrosion products easily promote the diffusion of Cl^- migrating from the 1# position. Therefore, the results of increasing corrosion area and decreasing maximum pitting depth were the synergistic results of accelerated general corrosion and combination of small pitting.

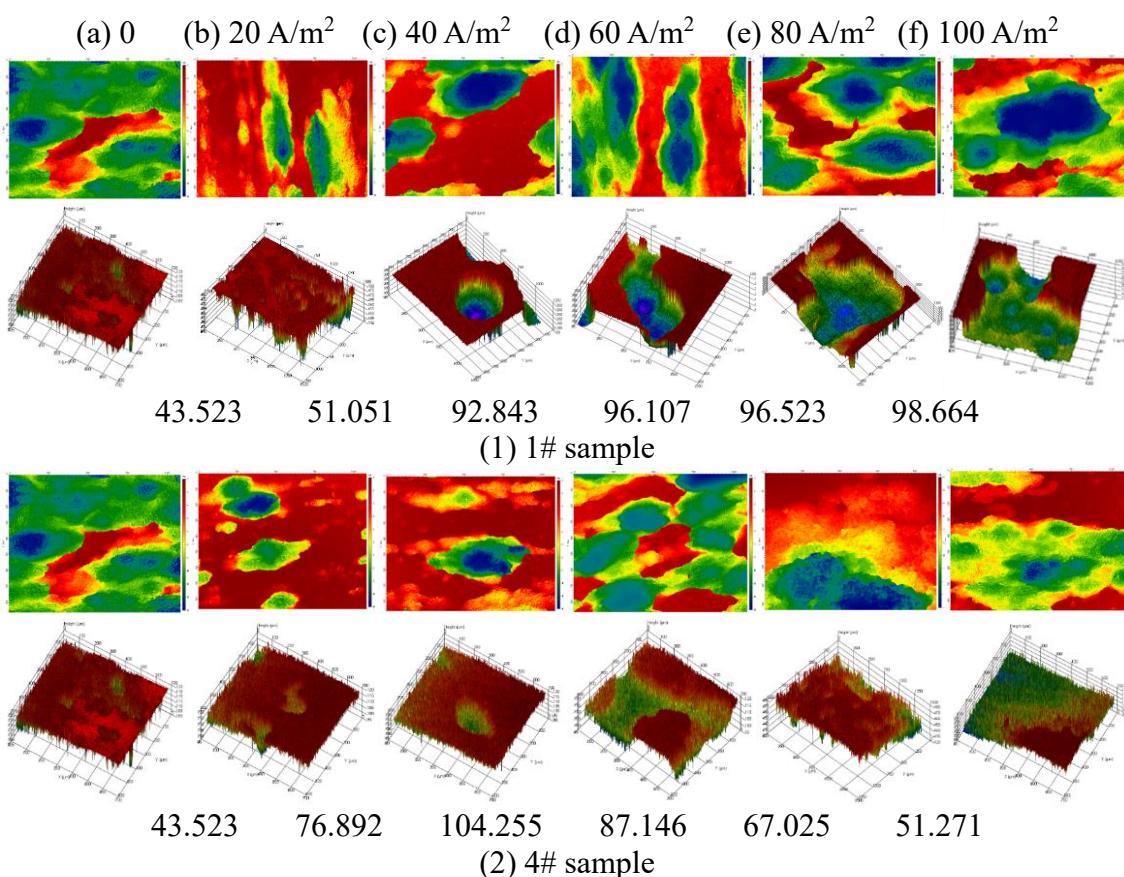


Figure 10. The corrosion morphology and maximum pitting depth of 1# and 4# samples under different conditions of CP current densities in 0-100 A/cm² in 3 wt.% NaCl solution at 20°C

4. CONCLUSIONS

Focusing on the shielding effect of crevice structure in bridge concrete on cathodic protection, this paper studied the corrosion behavior of HRB500 steel along the crevice structure in 3 wt.% NaCl

solution under different conditions of CP current densities through electrochemical experiments and corrosion morphology characterization. The mainly following conclusions were drawn.

(1) Under the condition of no cathodic protection, the self-corrosion potential (E_{sc}) of four samples at different positions was positively shifted with the increase of experimental time in 0-36 h, and the corrosion behaviors showed activation corrosion characteristics. The oxygen-difference cell began to be formed at 36 h and completed at 72 h, at which the E_{sc} of 1# and 2# samples was negatively shifted as cathode, while the E_{sc} of 3# and 4# samples was positively shifted as anode, and the E_{sc} of four samples basically remained unchanged.

(2) Under the different conditions of CP current density (I_{CP}) in 0-100 A/m², the corrosion behavior of 1# sample showed the activation corrosion characteristic, which changed from anode control to mixed control. At $I_{CP} = 20$ A/m² and 40 A/m², the corrosion current density of 1# sample was reduced by cathodic protection. With the continuous increase of I_{CP} , the hydrogen-evolution reaction of 1# sample occurred, and the corrosion morphology changed from general corrosion to pitting corrosion, while the maximum depth remained unchanged with an increasing corrosion area.

(3) Under the different conditions of CP current density (I_{CP}) in 0-100 A/m² applied on 1# sample, the corrosion behavior of 4# sample was controlled by the cathode reaction. With the increase of I_{CP} , the cathode control weakened. The corrosion morphology changed from pitting corrosion to general corrosion, and the maximum pitting depth reached 104.255 μm at 40 A/m², which was the synergistic results of accelerated general corrosion and combination of small pitting.

References

1. X. Cheng, J. Xia, R.J. Wu, W.L. Jin and C.G. Pan. *J. Build. Eng.*, 45 (2022) 103515.
2. B.V. Belleghem, M. Maes and T. Soetens. *Constr. Build. Mater.*, 310 (2021) 125187.
3. N.K. Prasad, A.S. Pathak, S. Kundu, P. Panchal and K. Mondal. *J. Mater. Res. Technol.*, 14 (2021) 582.
4. G.K. Glass, A.M. Hassanein and N.R. Buenfeld. *Corros. Sci.*, 39 (1997) 1451.
5. A. Goyal, E.K. Olorunnipa, H.S. Pouya, E. Ganjian and A.O. Olubanwo. *Constr. Build. Mater.*, 262 (2020) 120580.
6. N. Krishnan, D.K. Kamde, Z.D. Veedu, R.G. Pillai, D. Shah and R. Velayudham. *J. Build. Eng.*, 42 (2021) 102467.
7. L. Bertolini, F. Bolzoni, T. Pastore and P. Pedferri. *Cement Concrete Res.*, 34 (2004) 681.
8. F. Wang, J.X. Xu, Y. Xu, L.H. Jiang and G.X. Ma. *Constr. Build. Mater.*, 246 (2020) 118476.
9. W.H. Guo, J. Hu, Y.W. Ma, H.L. Huang, S.H. Yin, J.X. Wei and Q.J. Yu. *Corros. Sci.*, 165 (2020) 108366.
10. K. Ishii, H. Seki, T. Fukute and K. Ikawa. *Constr. Build. Mater.*, 12 (1998) 125.
11. A. Goyal, H.S. Pouya and E. Ganjian. *Constr. Build. Mater.*, 223 (2019) 1083.
12. E.Q. Zhang, Z. Abbas and L.P. Tang. *J. Constr. Build. Mater.*, 185 (2018) 57.
13. P.V. Bahekar and S.S. Gadve. *Constr. Build. Mater.*, 156 (2017) 242.
14. C. Christodoulou and R. Kilgour. *Corros. Mater.*, 39 (2014) 36.
15. C. Christodoulou, A. Sharifi, S. Das and C. Goodier. *Proc. Inst. Civ. Eng-Br.*, 167 (2014) 43.
16. J. Carmona, P. Garcés and M.A. Climent. *Corros. Sci.*, 96 (2015) 102.
17. J.C. Calero, M.A.C. Llorca and P.G. Terradillos. *J. Electroanal. Chem.*, 793 (2017) 8.
18. J. Xu and W. Yao. *Constr. Build. Mater.*, 23 (2009) 2220.

19. G.T. Parthiban, T. Parthiban, R. Ravi, V. Saraswathy, N. Palaniswamy and V. Sivan. *Corros. Sci.*, 50 (2008) 3329.
20. K. Wilson, M. Jawed and V. Ngala. *Constr. Build. Mater.*, 39 (2013) 19.
21. M.S. Anwar, B. Sujitha and R. Vedalakshmi. *Constr. Build. Mater.*, 71 (2014) 167.
22. J. Xu and W. Yao. *Constr. Build. Mater.*, 25 (2011) 2655.
23. J. García, F. Almeraya, C. Barrios, C. Gaona, R. Núñez, I. López, M. Rodríguez, A. Martínez-Villafañe and J.M. Bastidas. *Cement Concrete Comp.*, 34 (2012) 242.
24. E. Redaelli, F. Lollini and L. Bertolini. *Constr. Build. Mater.*, 39 (2013) 95.
25. G.F. Qiao, B.B. Guo, J.P. Ou, F. Xu and Z.H. Li. *Constr. Build. Mater.*, 119 (2016) 260.
26. R.B. Polder, G. Leegwater, D. Worm and W. Courage. *Cement Concrete Comp.*, 47 (2014) 69.
27. J. Orlikowski, S. Cebulski and K. Darowicki. *Cement Concrete Comp.*, 26 (2004) 721.

© 2022 The Authors. Published by ESG (www.electrochemsci.org). This article is an open access article distributed under the terms and conditions of the Creative Commons Attribution license (<http://creativecommons.org/licenses/by/4.0/>).